Paper ID 134

Measurements of the Turbulent Flow Environment on the Ground Below a Hovering Rotor

Jürgen Rauleder* J. Gordon Leishman†

Department of Aerospace Engineering
University of Maryland, College Park, MD 20742

Abstract

The vortical wakes produced by rotorcraft operating in ground effect induce high shear stresses and pressure forces on the ground, which can cause brownout conditions during landings or takeoffs in arid environments. The objective of the present work was to analyze the vortical and turbulent nature of the rotor flow as it interacted with a ground plane, and to better understand how the flow structures there may influence the process of sediment mobilization and uplift, ultimately leading to a better understanding of brownout. Detailed single-phase and dual-phase particle image velocimetry (PIV) measurements on a impermeable plane below a subscale hovering rotor were analyzed and compared to simpler, canonical flows such as a fully developed turbulent boundary layer and a steady wall jet. PIV measurements were obtained in the rotor wake and deep into the boundary layer region at the ground plane. The results have shown that the mean flow comprised certain features of a turbulent wall jet, but only in the expanding flow well downstream from the rotor. The instantaneous flow field at the ground closer to the rotor was very complex and contained the remnants of the blade tip vortices, the vortex sheets, and various small scale turbulence and eddies. These flow structures significantly affected the velocity field and the Reynolds stress distributions at the ground, which can both affect sediment mobilization and uplift. The quadrant analysis method was also employed to help understand the turbulent dual-phase flow at the ground. The results suggested that the quadrant analysis provides considerable insight into the conditions that can affect sediment mobility and uplift, and may help to establish a future predictive capability for brownout.

Nomenclature

A	Rotor disk area, $= \pi R^2$
DL	Disk loading, $= T/A$
r	Radial distance measured from rotor axis
R	Rotor radius
Re	Reynolds number, $= (u_{\max}\, y_{\max})/\nu$
T	Rotor thrust
u, v	Velocities in r and z directions, respectively
u', v'	Perturbation velocities in r and z directions, respectively
u_m, v_m	Mean velocities in r and z directions, respectively
$u_{\max}$	Maximum flow velocity
u_p, v_p	Particle velocities in r and z directions, respectively
u_τ	Friction velocity, $= \sqrt{(\tau_w/\rho)}$
u^+	Normalized wall-parallel velocity, $= u/u_\tau$
V_{tip}	Rotor tip speed
$y_{\max}$	Distance of maximum velocity from wall
z	Distance of rotor above ground plane
z^+	Normalized distance from ground, $= z(u_\tau/\nu)$
ν	Kinematic viscosity
ρ	Density
τ	Reynolds shear stress (in 2-dimensions), $= -\rho\,\overline{u'v'}$
τ_w	Wall shear stress
ψ	Blade azimuth

* Ph.D. Student. E-mail: **juergenr@umd.edu**

† Minta Martin Professor. E-mail: **leishman@umd.edu**

Presented at the 37th European Rotorcraft Forum, Gallarate, Italy, September 13–15, 2011.

Introduction

"Brownout" conditions occur when there is a sudden development of a dense dust cloud around a rotorcraft as it takes off, lands, or hovers over surfaces covered with loose sediment particles such as sand. Beside the effects of the suspended particles on blade erosion and mechanical wear, the intensity of the resulting dust cloud can cause severe visual obscurations and motion cue anomalies that affect a pilot's ability to safely fly the helicopter. The occurrence of brownout has been reported to be the leading cause of human factor-related helicopter mishaps in military operations [1], and civilian helicopters also suffer from the problem [2]. While sensor and avionics displays combined with operational tactics (i.e., flight path management) have helped somewhat to reduce the frequency of brownout-related mishaps, in the longer term an improved understanding of the physical factors that influence the occurrence of brownout and the exploration of strategies to mitigate it, will be critical for ensuring safe and cost-effective rotorcraft operations.

Underlying the physics of the problem of brownout is unsteady, turbulent, dual-phase fluid dynamics. The dual-phase nature of the problem arises because the fluid (or carrier) phase produced by the rotor wake creates a dust particle (or dispersed) phase; see Fig. 1. Recent experimental studies have begun to expose the details of the flows on a ground plane below a hovering rotor; see Lee et al. [3] and Milluzzo et al. [4], the latter obtaining measurements deep into the boundary layer at the ground. Such flow fields contain the remnants of the tip vortices and vortex sheets from the rotor blades, as well as various small scale turbulence and eddies; see Fig. 2. Measurements have also been made of the dual-phase heterogeneous flow environment from a sediment bed below a rotor [5–7]. High surface shear stresses combined

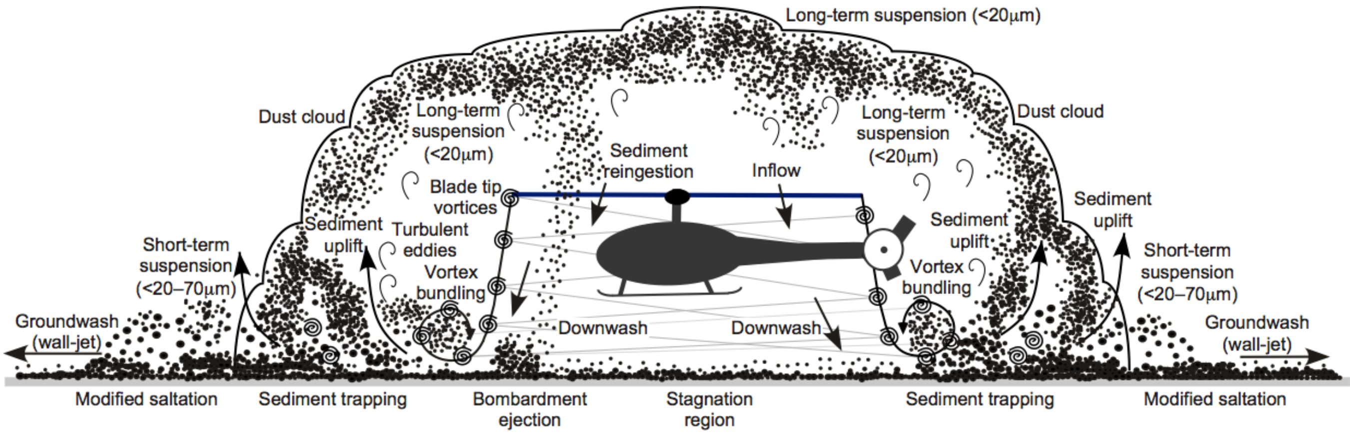

Fig. 1: Schematic showing different modes of particle uplift and particle motions generated by a helicopter above a mobile sediment bed.

with low pressures and the unsteady upward flow velocities induced by the tip vortices lead to the trapping of sediment particles, uplifting them from the bed. Any suspended particles are then convected away by the highly three-dimensional, turbulent, unsteady flow. The smaller and lighter particles trapped in the stronger vortical flow regions may be recirculated and bombarded back onto the sediment bed, ejecting more particles in the process and rapidly intensifying the total quantity of suspended particles in the flow. If sufficient particle concentrations build up, thereby changing the mass density of the flow, then the carrier itself may be modified (i.e., the problem becomes two-way coupled). Factors compounding the transport characteristics include particle-particle interactions (i.e., four-way coupling) and the morphology of the sediment bed itself (i.e., through deflation, deposition, and dune formation).

Modeling of the brownout problem is obviously challenging, but ambitious simulations have been attempted [8–16]. Besides the complexity of the rotor flow itself, simplified assumptions and approximations must be used to model particle pickup and transport from the underlying sediment bed. Most such pickup models are semi-empirical integral descriptions based on the assumptions of steady, uniform, fully turbulent boundary layer flows [17, 18]. However, in light of the growing experimental evidence, such models are more questionable for the nonequilibrium flows found below the rotor. In steady, uniform boundary layers, the effects on particle mobility can be characterized by the shear stresses on the bed because the statistical distributions of the turbulent fluctuations scale with the shear velocity [19]. Because the lift and drag forces that mobilize sediment particles are produced by the integrated effects of the instantaneous fluid velocities on the particles, the mean rate of sediment transport in such flows can also be characterized by the shear stress. In nonuniform or unsteady flows, however, the turbulent fluctuations do not necessarily scale with the local bed shear stress. In fact, measurements [19–22] have already shown that nonuniformities in the flow can produce substantial changes in the near-bed turbulence field that, in turn, play an important role in the movement and entrainment of particles into the flow. Consequently, the predicted motion of sediment particles are likely to be inaccurate if methods developed for uniform flows are used for brownout studies.

The objectives of the present work were to better understand the processes of particle uplift from an underlying sediment bed below a rotor from the analysis of both single-phase and dual-phase flow measurements. Even in the absence of sediment particles, it is essential to understand the fluid dynamic characteristics of the complex turbulent flow at the ground. A longer term goal is to develop and validate mathematical models for sediment mobility and uplift that are applicable to rotor flows. To this end, the role of both concentrated vorticity and turbulence in the flow must be carefully investigated as it influences the motion of the sediment particles on the ground below the rotor. In the present work, particle image velocimetry (PIV) measurements on a ground plane below laboratory-scale hovering rotors were analyzed, including the distribution of Reynolds shear stresses. The results were compared to those of a fully developed turbulent boundary layer and to a steady wall jet. The flow structures below the rotor were noted to significantly affect the velocity excursions and the Reynolds stress distributions at the ground, which in turn will influence sediment mobilization and uplift. The quadrant analysis was also employed to help understand the turbulent dual-phase flow near the ground.

Fluid Mechanics of a Rotor Wake Near a Ground Plane

As previously discussed, the physical problem of brownout is, fundamentally, an unsteady, dual-phase, fluid dynamics problem. When a rotor operates in ground effect, the rotor wake impinges on the ground and generates unsteady shear stresses, secondary vortical structures, turbulence and transient velocity excursions, all of which are contributors to the mechanisms of sediment transport and uplift, particle entrainment or suspension, and ultimately to the development of a brownout cloud. A prerequisite to understanding this problem is obviously to understand the fluid dynamics of the rotor wake as it approaches the ground.

Detailed measurements have been made of the flow on a ground plane below a rotor operating in hover [4], which have been further analyzed in the present work. Particle image velocimetry (PIV) was used to make measurements of the flows from a single-bladed rotor of radius of 0.408 m and a blade chord of 44.5 mm with a standard tip, operating above a circular plane of 1.626 m diameter. The ground plane was positioned one rotor radius below the rotor plane of rotation to simulate ground effect conditions; see Milluzzo et al. [4].

Figure 2 shows the essential flow features in the rotor wake developing in ground effect by means of a flow visualization

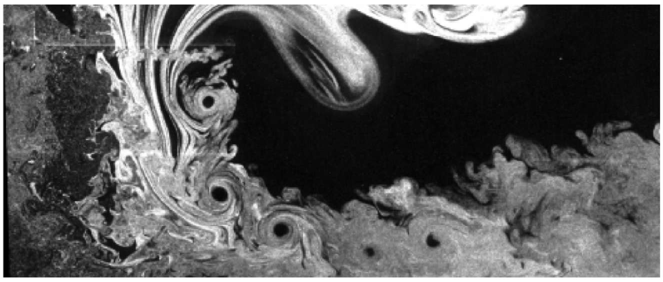

(a) Flow visualization image

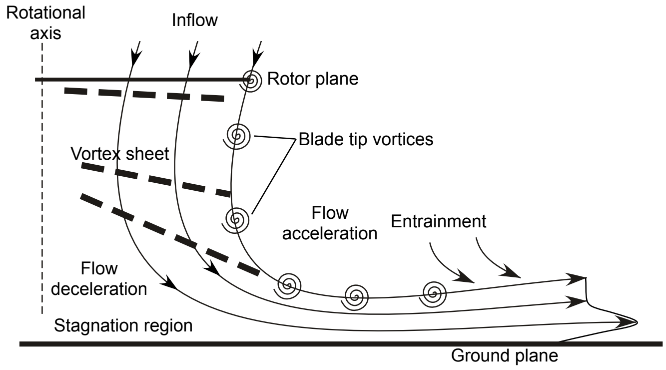

(b) Schematic of the flow

Fig. 2: Flow features in the rotor wake developing in ground effect shown by: (a) flow visualization, (b) corresponding schematic of the flow characteristics.

image and a corresponding schematic of the flow field. Having passed through the rotor, the flow is decelerated as it approaches the ground plane. However, because the flow has to turn rapidly from a predominantly axial flow (i.e., downward) to a radial flow (i.e., parallel to the ground plane), it is accelerated again after this 90° turn. As more and more flow from the low velocity region outside the rotor wake becomes entrained, the radial stream becomes thicker, and a turbulent wall jet starts to develop over the ground plane.

Two important features of this flow are the blade tip vortices and the turbulent vortex sheets; these flow structures are apparent in the flow visualization image in Fig. 2. The tip vortices convect along the slipstream boundary; in the flow visualization image they manifest as dark voids that are caused by the action of centrifugal forces on the submicron seed particles. The vortices are stretched lengthwise as they interact with the ground, a process that intensifies their vorticity. A turbulent vortex sheet is also formed behind the blade; Ramasamy et al. [23] have performed measurements of this flow structure. Such vortex sheets result from the merging of the boundary layers on the upper and lower surfaces of the blade and contain counter-rotating or Taylor–Görtler vortices; these are caused by the streamline curvature of the boundary layer on the blade [23, 24].

After these vortical flows have been trailed from the rotor, they convect downstream toward the ground plane and become part of the developing wall jet-like flow at the ground, which leads to a significant increase in the overall turbulence there. The convection and subsequent ingestion of the turbulent vortex sheets into the developing flow at the ground has been examined by Sydney et al. [7] using time-resolved flow visualization and PIV measurements. Also, interactions between the flow structures appear to create secondary flows, such as localized zones of flow separation or secondary vorticity, which contribute further to the flow complexity and the unsteady aerodynamic environment on the ground below the rotor.

Results and Discussion

Flow Field at the Ground

Understanding the detailed fluid dynamic characteristics of the complex rotor flow at the ground is important because it is a prerequisite to establish and validate mathematical/numerical models for bedload transport and particle uplift models that are applicable to such rotor flows. For these purposes, the instantaneous characteristics of the flow and the velocity excursions at the ground are important [4,7,25]. Representative profiles of the time-averaged and phased-averaged (periodic) wall-parallel velocity at three downstream distances from the rotor centerline from the measurements of Milluzzo et al. [4] are shown in Fig. 3, and appear very similar to a developing turbulent wall jet. The phase-averaged results were ensemble averaged over consecutive PIV flow field realizations with the rotor blade in the same azimuthal position, ψ (see later).

Because of the unique flow features in the rotor wake (see Fig. 2), the resulting transient excursions of the flow velocities at the ground also contain significant turbulence levels and Reynolds shear stresses, as well as the production of secondary vortical flows. These turbulent flows, which mainly have their initial source in the tip vortices and vortex sheets, have more pronounced correlative structures compared to what would be found in simpler flows such as channel or pipe flows. However, after ensemble averaging is performed and only the mean quantities of the flow are resolved, these distinct aspects of the flow are attenuated. Therefore, in the present work special attention was given to the temporal flow fluctuations and the Reynolds stresses in the rotor wake as it approached the ground.

The influence of the blade tip vortices on the flow at the ground plane become apparent when focusing on the boundary layer region directly below a passing tip vortex, an instantaneous realization being shown in Fig. 4. These results show the locally higher induced flow velocities at the ground induced by the vortex when it convects by a fixed point on the ground. There is also a thickening of the boundary layer on the ground as a consequence of the adverse pressure gradient produced by this vortex flow. In fact, the results showed that the boundary layer immediately below the vortex was in a state of incipient separation; it can be expected that the flow may separate for vortices of sufficient strength. Flow separation can affect the process of sediment uplift and entrainment, as shown for channel and riverine flows by Nelson [19] and for a rotor flow by Johnson et al. [6].

Figure 4 shows the detail necessary to better assess the boundary layer state and to sufficiently resolve the near-wall flow. Measurements in this case were made down to a height of only $0.001R$ above the ground plane. Below that height, issues associated with surface reflections of the incident laser light sheet became problematic and the PIV measurements

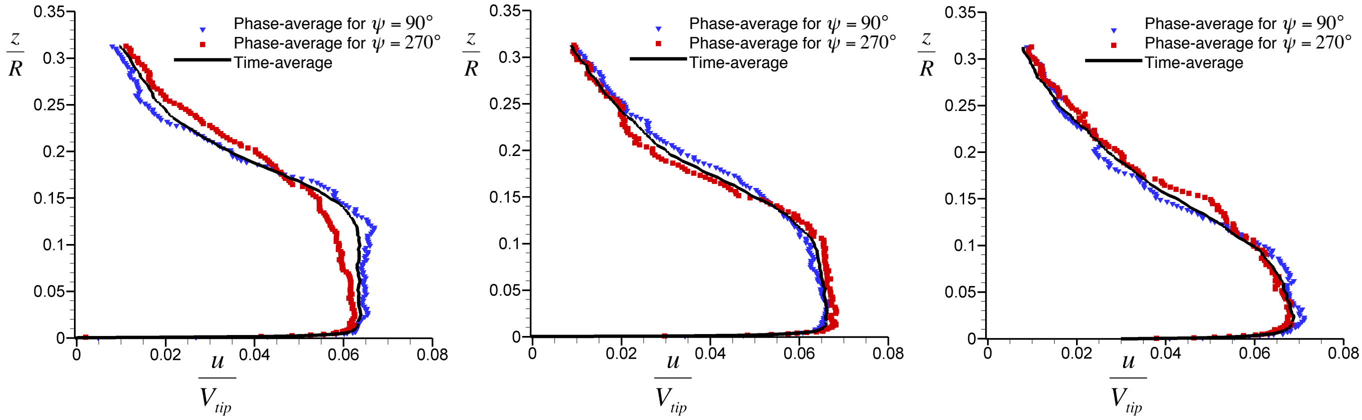

(a) $r/R = 1.29$ (b) $r/R = 1.40$ (c) $r/R = 1.60$

Fig. 3: Examples of the time-averaged and phase-averaged wall-parallel flow velocity on the ground plane at three downstream distances from the rotor. Data processed from [4].

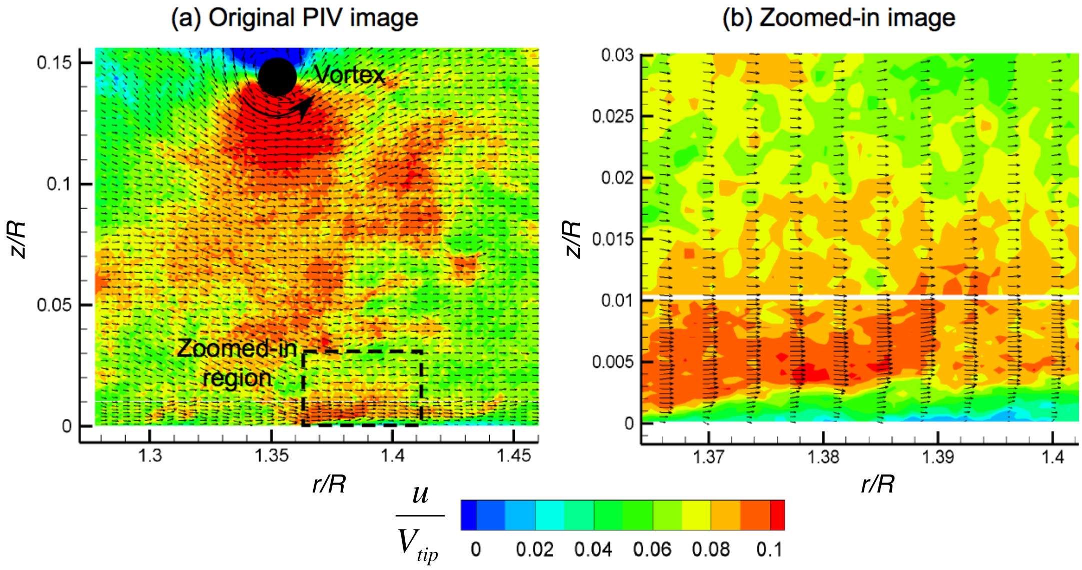

Fig. 4: Example of the instantaneous flow details resolved near the wall surface. Instantaneous flow vectors are plotted on background contours of wall-parallel velocity. Area of detailed image shown by the dashed line.

contained more errors. A higher spatial resolution was actually obtained compared to what is shown in this figure; to avoid image congestion only every fifth vector is shown in the horizontal direction although every vector is shown in the wall-normal direction up to $z/R = 0.01$.

Reynolds Shear Stresses

Figure 4 shows that as the blade tip vortices approached the ground they induced transient increases in the wall-parallel flow velocity components. This effect, in turn, generates considerably larger shear stresses. Particle motion arises, at least in part, from the shear stresses produced on the sediment bed by the flow [26]. When a certain threshold condition is reached, particles are initially transported downstream into saltation and can then be entrained and uplifted into the outer flow by eddies or vortices [7]. Because of the highly turbulent flow generated by a rotor, the Reynolds stresses are, in fact, the dominant source of stresses in this case. The fidelity of the PIV measurements was such that it allowed for the fluctuating part of the flow velocities to be extracted, which were then used for the computation of the Reynolds shear stresses.

The Reynolds shear stresses (in two-dimensions) are

$$\tau = -\rho\, \overline{u'v'}, \tag{1}$$

with the perturbation velocities u' in the r direction (i.e., radial perturbation velocity) and v' in the z direction (i.e., axial or wall-normal perturbation velocity). Performing a Reynolds decomposition, the perturbation velocities are

$$u'_{i,j} = u_{i,j} - u_{m_{i,j}}, \tag{2}$$

$$v'_{i,j} = v_{i,j} - v_{m_{i,j}}. \tag{3}$$

In this case, $u'_{i,j}$ is the perturbation velocity at a single interrogation point, $u_{i,j}$ is the instantaneous velocity at this point in space, and $u_{m_{i,j}}$ is the average u velocity at this point. The average velocity components were calculated using

$$u_{m_{i,j}} = \frac{1}{N}\sum_{k=1}^{N} u_{i,j}(k), \tag{4}$$

which in this case is for the u component, where N is the number of PIV realizations at a given blade position. This method of averaging the flow properties is called phase-averaging. A similar equation holds for the v component.

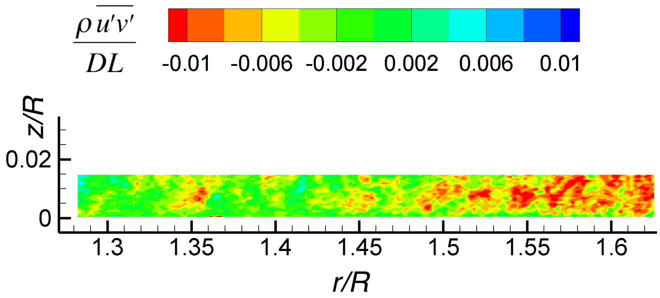

Fig. 5: Reynolds shear stress distribution in the boundary layer region below the rotor at the ground normalized by rotor disk loading, *DL*.

A representative Reynolds shear stress distribution is shown in Fig. 5 for measurements made in the boundary layer region. Notice that the height above the ground z and the radial distance from the rotational axis r are both normalized by the rotor blade radius R. The wall-normal distance shown is approximately 2% rotor radius, corresponding to a physical distance of only 8 mm. From the measurements, it was apparent that the tip vortices produced complex spatial variations in the shear stresses. The region with the highest turbulent shear stresses was located where the tip vortices were closest to the ground plane, also inducing the highest velocity fluctuations in the flow. However, the results shown in Fig. 5 are clearly different to those of a fully developed turbulent boundary layer, where the spatial distribution of Reynolds shear stress is known to be approximately linear when moving away from the wall [27].

Figure 6 shows further details of the Reynolds shear stresses as the flow develops on the ground plane, the data being extracted at three downstream radial locations r/R = 1.29, 1.40, and 1.60. Notice that the boundary layer region (shown previously in Fig. 5) in the wall-normal direction is only a small fraction of that shown in Fig. 6. It is apparent that the maximum Reynolds shear stresses coincided with the slipstream boundary between the accelerated flow inside the rotor wake and the more quiescent outer flow. The tip vortices travel downstream along this slipstream boundary (see Fig. 2), generating additional turbulent stresses as they do so. This behavior manifested in a pronounced peak in the Reynolds stresses seen at all radial distances downstream from the rotor. Notice the various other significant excursions in the shear stress profile (Fig. 6). These excursions are a consequence of the aperiodicity in the rotor flow and other flow features such as the vortex sheets that are also convected and entrained into the developing wall jet-like flow.

Notice that as this wall flow developed, the turbulent shear stresses changed sign and became negative near the wall (see Figs. 6(b) and 6(c)), an observation also made with steady wall-jet flows [28, 29] that can be explained from Prandtl's mixing-length theory. As the fluid passes along the wall in turbulent motion, the fluid elements retain their streamwise momentum. The turbulent motion causes a fluid element to be displaced from a layer nearer to the wall to a layer further away from the wall (but still within the boundary layer). Because the fluid element keeps its original momentum, its streamwise velocity u is smaller than the streamwise velocity that prevails at the new location. (The wall-normal perturbation velocity v' is defined as positive in the direction pointing away from the wall.) The fluid particle has an excess velocity in the wall-normal direction and, therefore, it caries a positive fluctuating velocity component v'. Because this fluid element also had a smaller instantaneous u velocity component than the prevailing elements in its new layer (i.e., lower than the mean value of streamwise velocity u_m), a mostly negative fluctuating velocity component u' is produced. Therefore, the product $(u'v')$ is negative. For a fluid element moving in the opposite direction, i.e., toward the wall $(v' < 0)$, it carries an excess velocity in the streamwise direction, giving rise to mostly a positive streamwise fluctuation velocity component $(u' > 0)$. "Mostly" in this context means that the appearance of fluid elements for which u' has the opposite sign of v' is much more frequent, therefore, the temporal average $\overline{u'v'}$ is negative. For a turbulent boundary layer, the average value of $\overline{u'v'}$, therefore, is always negative, while for a wall jet it changes sign from negative to positive at the approximate wall-normal position of the velocity maximum because of the change in the sign of the slope of the wall-parallel velocity profile.

It should be noted that beside the similarities in the flows in comparison to simpler wall-bounded flows as previously pointed out, there were also significant differences in the radial and wall-normal distribution of Reynolds stresses for the rotor flow. For the purposes of this paper, these two more traditional, simpler flow problems are hereafter referred to as the canonical flows.

Boundary Layer Profile

In integral models used to represent bedload transport and particle mobility, assumptions have to be made about the nature of the boundary layer over the ground. Therefore, it is critically important to know the structure and length scales of the boundary layer from measurements. Various approximations and assumptions have been used by numerical simulations of rotor flows in ground effect, and for sediment transport models (where the viscous portion of the flow at the ground is important). However, most assumptions have not yet been validated using actual measurements obtained from rotor experiments. To this end, measurements of the boundary layer velocity profile on the ground plane below the rotor were examined in detail.

For the furthest downstream distance shown in Fig. 6(c), notice the pronounced second local (negative) maximum in the Reynolds stresses and the subsequent steep decrease in magnitude as the wall is approached, which suggested that the measurement points closest to the wall were within the viscous sublayer. Viscous forces are predominant in this region of the boundary layer. Therefore, the Reynolds stresses decrease here and become almost negligible compared to elsewhere in the flow.

To better assess the state of the boundary layer and its length scales, the mean velocity profile was plotted in wall coordinates. Figures 6(c) and 7 suggest that the four or five measurement points closest to the wall were within the viscous sublayer. The values of u^+ were not equal to z^+ in this region, which may be attributed to an under-developed boundary layer and/or to the unique features comprising the rotor flow. However, as z^+ approaches about 30 wall units, the flow transitions to a more logarithmic velocity profile, i.e., the logarithmic law of the wall. This finding is important because it has implications on the modeling of the rotor flow at the ground, as well as for particle mobility and uplift models

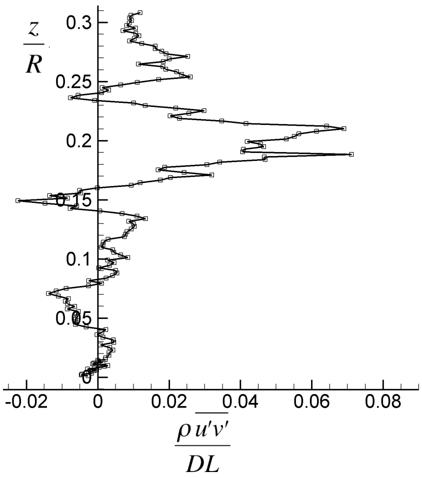

(a) $r/R = 1.29$

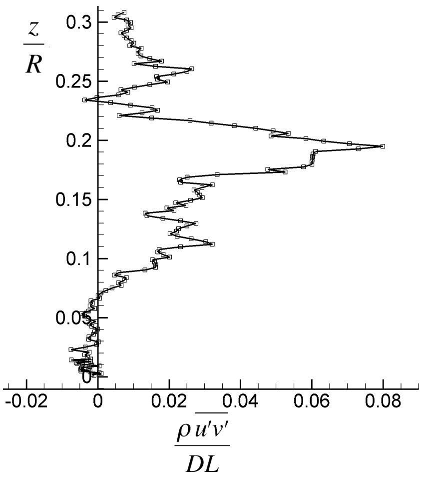

(b) $r/R = 1.40$

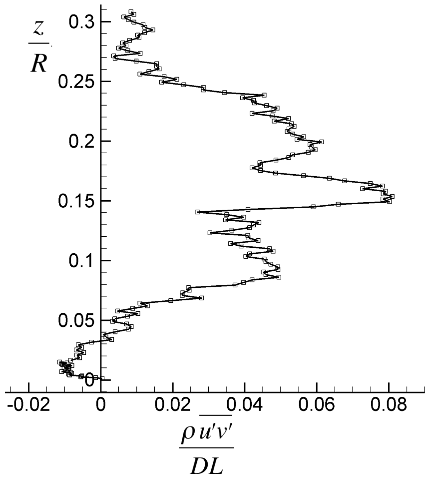

(c) $r/R = 1.60$

Fig. 6: Measured Reynolds shear stress profiles at several downstream distances from the rotor normalized by rotor disk loading, *DL*.

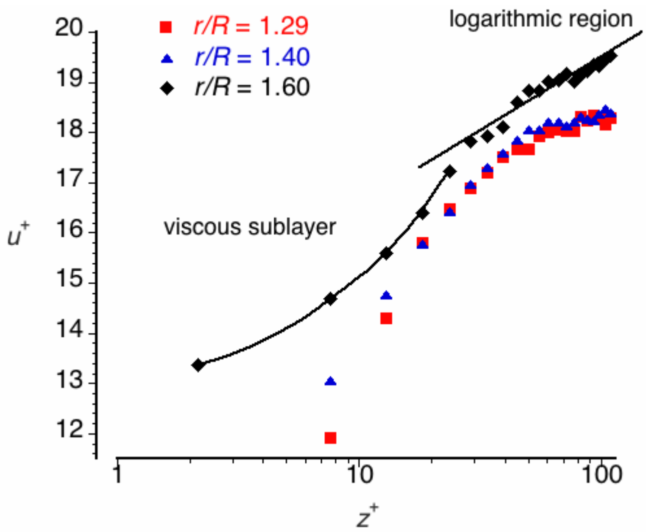

Fig. 7: Semi-logarithmic plots of the wall-parallel velocity profiles in terms of wall coordinates.

where a velocity profile at the wall may have to be prescribed. The measurements further downstream at least, have revealed the approximate wall-normal expansion of the viscous sublayer and validate the use of a logarithmic velocity profile between the viscous portion of the flow and the fully turbulent outer flow. The same conclusion, however, cannot be drawn for wall locations closer to the rotor.

Another interesting finding is that the mean velocity profile parallel to the wall below the hovering rotor (very close to the ground plane) appears to be similar to that of a fully developed turbulent boundary layer or the inner layer of a turbulent wall jet, which are qualitatively the same [30]. However, this observation is only true for the flow well downstream from the rotor. For the turbulent boundary layers produced by the canonical flows, the thickness of the viscous sublayer is in the range of $z^+ = 5$ to $z^+ = 30$, depending on the Reynolds number of the flow. Therefore, a thickness of $z^+ \approx 30$ that was measured for the rotor flow is in good agreement with these canonical flows. The Reynolds number of the mean rotor flow at the ground at $r/R = 1.60$ was $Re = 3{,}000$ based on the maximum of the wall-parallel velocity profile, $u_{\max}$, and the wall-normal distance from the wall where this velocity maximum occurred, $y_{\max}$, as the characteristic length.

Turbulence Intensities of the Single-Phase Flow

Although a good level of agreement with the canonical flows was seen for the mean velocity profiles at the wall, this is not the case for the Reynolds stresses close to the wall; see Fig. 8. These differences arise, in part, because the wall-parallel mean velocity distribution scales with the Reynolds number, however, the turbulent fluctuations (i.e., the Reynolds stresses) do not; see Wyganski et al. [30]. Furthermore, when ensemble averaging is performed, the temporal velocity fluctuations induced by the vortical structures are removed in the mean velocity profile, and what is left is essentially the profile of a turbulent wall jet; see Figs. 3 and 7.

Advection of multiple regions of vorticity (i.e., coherent structures such as tip vortices), is a highly nonlinear process. Therefore, even PIV realizations taken at the same blade position (i.e., if used to perform phase-averaging) can contain variations in the positions of the vortices, especially at older wake ages further downstream of the rotor. Under such conditions, any form of ensemble averaging of the measurements can remove the coherence that is present in the flow [31]. Therefore, special attention was given in the present work to the instantaneous fluctuating velocity components and the associated turbulent Reynolds stresses.

It may be argued that the Reynolds stresses themselves are based on an ensemble average. Through the ensemble averaging involved in the calculation of the Reynolds stresses, the aperiodic flow at the ground appears, even in terms of the Reynolds stress distribution, similar to that of a turbulent wall jet. Because of this aperiodicity, some of the flow structures unique to the rotor flow appear to rapidly lose their coherence. Therefore, an instantaneous realization of the turbulent velocity fluctuations in radial and wall-normal direction, u' and v', may be more revealing than the Reynolds shear stresses themselves. Although Reynolds-averaging techniques do not explicitly account for coherent motions in the turbulence, some form of instantaneous organization is apparent even in the averaged terms. Otherwise, the $-\rho\overline{u'v'}$ term (i.e., the most important closure term for the incompressible RANS equations) would be zero if the boundary layer turbulent motions were purely random without preferred correlations between the velocity components [32].

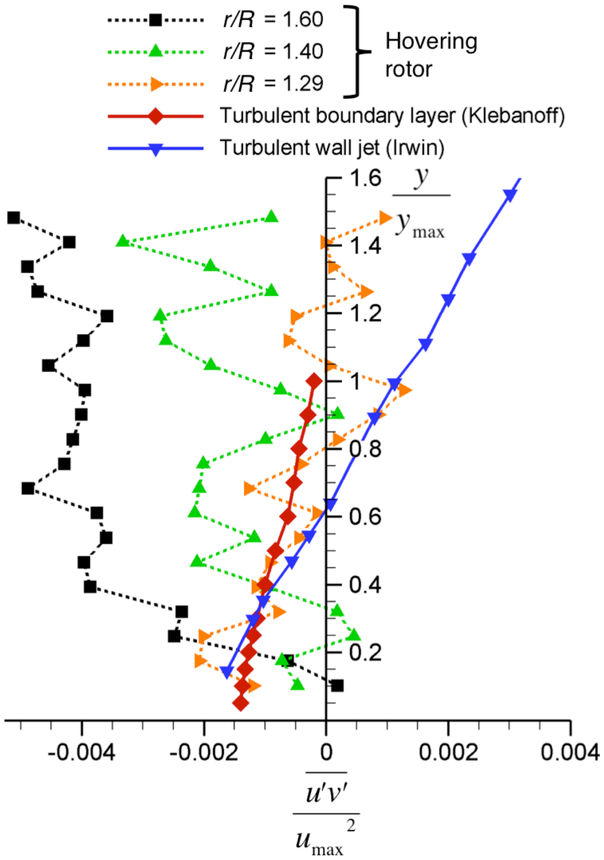

Fig. 8: Comparisons of the boundary layer flow in terms of Reynolds shear stress $\overline{u'v'}$ measured at the ground below a hovering rotor to the canonical flows.

In Fig. 8, the flow measurements on the plane below the rotor are compared to measurements obtained by Klebanoff [27] for the fully developed turbulent boundary layer, and by Irwin [29] for a turbulent wall jet. As it is conventional for wall jets, the turbulent shear stress $\overline{u'v'}$ was normalized by the local maximum of the wall-parallel velocity component u_{max}, and the wall-normal distance y was normalized by the distance from the wall at this local velocity maximum, y_{max}. For the turbulent boundary layer, u_{max} is the free-stream velocity of the outer flow and y_{max} is the mean boundary layer thickness, respectively. It should be noted that the measurements for these canonical flows were not conducted at the same Reynolds number, which has implications on the turbulence fluctuations and, therefore, on the Reynolds stresses.

The thickness of the viscous sublayer, as well as the extension of the log law region of the boundary layer at the wall, depend on the Reynolds number [33]. Comparing the distributions shown in Fig. 8 for the turbulent wall jet to those shown in Fig. 6(c) for the rotor flow, suggests that different length scales are involved with the rotor flow. The distance from the wall and the shear stress were normalized by the local length and velocity scales, repsectively. Nevertheless, at the same normalized distance from the wall, the measurement points closest to the wall (below $0.4\,y_{max}$) were in the viscous sublayer for the rotor flow (also see Fig. 7), while they were well above it in the turbulent wall jet measurements [29]. Likewise, the point where the Reynolds shear stresses changed sign was located much further away from the wall for the measurements below the rotor (see Fig. 6(c)), compared to the wall jet measurements. Also, for lower Reynolds numbers, the organized turbulent motions in a wall-bounded flow extend further away from the wall and lead to a stronger contribution to the Reynolds shear stresses, as was reported by Antonia et al. [34]. For these reasons, the different length scales obtained may be, in part, an artifact of the different Reynolds numbers of the experiments in this case.

The higher Reynolds shear stresses produced in the near-wall region, especially further downstream from the rotor, resulted primarily from the wall-parallel perturbation velocity, u', which is the predominant of the velocity fluctuations at the ground. The action of the tip vortices increased the velocity in wall-parallel direction, as shown in Fig. 4, and the magnitude of Reynolds shear stresses increased there as well. The results obtained further downstream at $r/R = 1.60$ showed the highest stresses because the tip vortices were closest to the ground, also inducing the highest instantaneous velocity excursions into the flow. At this radial location it was apparent that below $0.2\,y_{max}$, the Reynolds shear stress was lower compared to the canonical flows. This outcome was attributed to the fact that at $r/R = 1.60$, the last measurement points at the wall were within the viscous sublayer (see Fig. 7), where the turbulent stresses are suppressed. Irwin [29] and Klebanoff [27], however, could not obtain measurements close enough to the wall to penetrate the viscous sublayer.

Notice also the linear slope in the Reynolds shear stress profile with distance from the wall for the canonical flows in Fig. 8 that is not seen with the rotor flow. This outcome, again, can be attributed to the more complex flow environment in the near-wall flow below the rotor. The canonical flows obviously do not contain regions of concentrated vorticity nor do they include structures like the turbulent vortex sheets (described previously) trailed from the rotor blades. It can be seen from Figs. 5, 6 and 8 that there were significant small and large scale fluctuations in the Reynolds stresses in the boundary layer region as well as in the outer flow, which are not present in the canonical flows.

Dual-Phase Flow at the Ground

The results from the measurements shown thus far were from a single-phase flow experiment (i.e., without sediment particles), and have revealed many interesting characteristics of the unsteady flow below the rotor at the ground plane, which may also be important for validating numerical simulations. Further analysis of such detailed fluid flow measurements may help to understand where sediment particles are likely

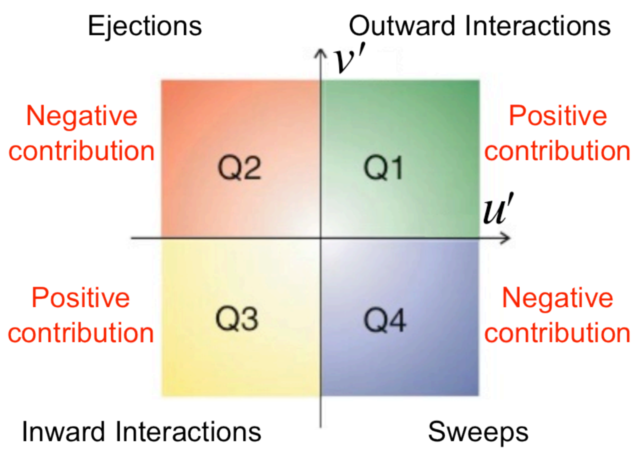

Fig. 9: A quadrant map showing the four types of motion (turbulence events) belonging to the quadrants and their contribution to the Reynolds shear stresses $\overline{u'v'}$.

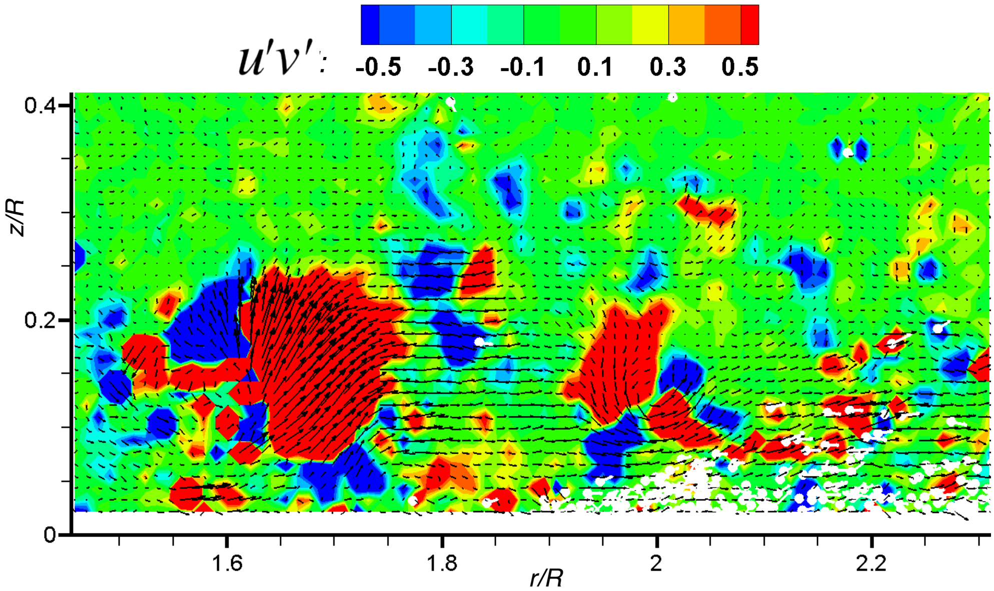

Fig. 10: Dual-phase flow realization showing instantaneous velocity vectors of the carrier and dispersed phases on a background contour of the shearing component of the instantaneous fluctuation velocities.

to become mobilized and uplifted through the action of the shear stresses and/or the direct action of vortices. However, from the single-phase experiments alone, no definitive conclusions can be drawn about sediment mobilization or uplift, and to this end, dual-phase measurements are needed. Such experiments are possible but extremely challenging [6, 7, 20]. Depending on the experimental configuration, it is not always possible to perform such experiments with sediment particles of the needed size and/or the required scaling parameters. However, if it can be concluded from a single-phase flow experiment where and why sediment particles are likely to become mobilized and uplifted, this may yield an interesting new predictive capability for brownout.

To this end, a method called the "quadrant analysis" as developed by Wallace et al. [35] has been explored in the present work. This method is based around observations of sequences of discrete turbulence events in the wall-bounded turbulent flows. Wallace et al. [35] found that there were four kinds of turbulence events, namely sweeps, ejections, outward and inward interactions. The quadrant analysis is based on the correlative structure of the perturbation velocities u' and v', which have been described previously. The four types of motion are classified by the signs of the perturbation velocities, u' and v'. The measurements are then plotted in a quadrant map, as shown in Fig. 9. The quadrant map essentially shows the main directions of the turbulent momentum transfer relative to the bulk movement of the fluid.

The interactions between sediment motions and the turbulence structure of the carrier phase, and how they correlated to these four turbulence events, has been studied by Nelson et al. [19] for riverine flows. While there are obviously significant differences in the time scales, turbulence levels, Reynolds numbers and spatial dimensions between simple channel flows or river bed flows and the brownout problem, the quadrant analysis may also yield an interesting approach for examining the sediment uplift, entrainment, and suspension mechanisms that contribute to the development of a brownout dust cloud. To this end, the dual-phase PIV data of Sydney et al. [7] have been analyzed in the present study. In this experiment, the plane of rotation of a small, two-bladed rotor system was located one rotor radius above a ground plane that was covered with a sediment bed of characterized glass mircospheres; see [7] for details of the experimental setup and the particles used.

Figures 11(a) and 11(b) show flow regions very close to the bed, which are obviously critical regions for sediment transport and uplift. These PIV measurements are taken at the same instance as those shown in Fig. 10; in fact, it is the same image but in this case it details the region very close to the ground/sediment bed. Figure 11(a) shows the upstream portion of the flow at the ground, while Fig. 11(b) shows the downstream portion of Fig. 10 for a small wall-normal distance where most of the sediment is mobilized. Closer to the ground plane, laser reflections from the ground/bed became an issue and did not allow for accurate flow measurements.

Analyzing the dual-phase flow at the ground below a hovering rotor from this perspective is extremely useful because the flow environment is dominated by the turbulence, and the motion and uplift of dust particles strongly depends on the fluctuating part of the velocity field rather than on the time-averaged flow field [7, 25]. It is clear that the instantaneous flow field also includes significant turbulence and eddies of various scales and is dominated by velocity fluctuations, as can be seen in the realization showing the complete region at the ground; see Fig. 10. In this figure, the background contour is based on the instantaneous shearing component of the velocity fluctuations. The classic four-lobed pattern associated with analyzing coherent vortex structures in a Cartesian coordinate system [23, 31] can be observed at $r/R = 2$, with the vortex core located at a height of $z/R = 0.12$ above the ground plane. Furthermore, significant local maxima in the shearing components are apparent near the ground, which stem from the smaller, less coherent vortical structures, but which clearly also give rise to significant shear stresses.

From the detailed regions near the ground, the fluctuation velocities of the carrier phase and the particle velocities of the heterogeneous dispersed phase were obtained and plotted in the form of quadrant maps; see Figs. 11(c) and 11(d) for the fluctuation velocities, and Figs. 11(e) and 11(f) for the particle velocities. Notice the correlative structure of the fluctuat-

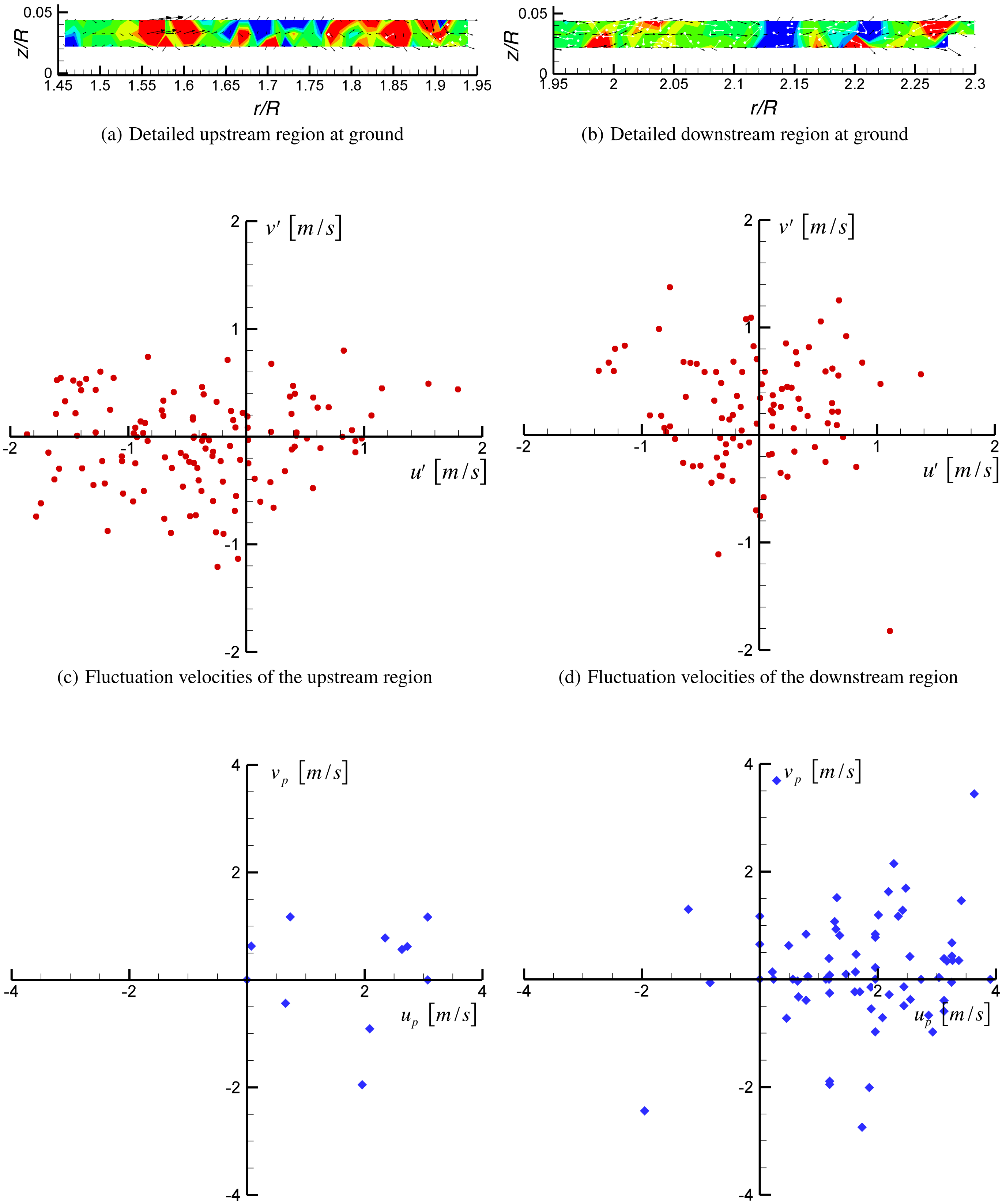

(a) Detailed upstream region at ground

(b) Detailed downstream region at ground

(c) Fluctuation velocities of the upstream region

(d) Fluctuation velocities of the downstream region

(e) Instantaneous particle velocities upstream

(f) Instantaneous particle velocities downstream

Fig. 11: Dual-phase flow realization detailing the region just above the sediment bed for upstream (a) and downstream (b) portions of the flow. Corresponding quadrant plots showing the fluctuation velocities of the carrier phase, (c) and (d), and the corresponding instantaneous particle velocities for these regions, (e) and (f), respectively.

ing velocity components. However, the correlations in $(u'v')$ do not show the characteristic behavior of the near-wall flow that is found with the canonical flows. This result reflects the temporal and spatial structures of the impinging tip vortices and the other significant vortical flow features that comprise the rotor wake as it interacts with the ground. Notice that upstream, despite the intense upwash region at $r/R = 1.7$ shown in Fig. 10, there are only few sediment particles uplifted to an elevation above the bed that allows them to be measured.

As for the quadrant plot showing the fluctuation velocities for the region upstream (Fig. 11(c)), the carrier phase shows primarily inward interactions and ejection motions, which are both known to be individually the least significant of the four turbulent motions to affect sediment pickup. The quadrant plot for the carrier phase in the downstream region (Fig. 11(d)) shows that the predominant turbulence events here are outward interactions and ejections. The former are the most powerful motions affecting sediment transport [19]. These motions are rare in standard channel and boundary layer flows, but are clearly significant in certain portions of the flow at the ground below the rotor, as observed in the present work. Ejections are known to be responsible for particle suspension. This finding from simple channel flows seems to be applicable to rotor flows as well; for the region of interest shown in Fig. 11(b), many particles have already been uplifted and entrained into the flow and are subsequently suspended downstream. Not only that, but the quantity of mobile particles in the flow downstream is larger compared to the regions further upstream. These particles also carry a lot of momentum, primarily in the streamwise and upwards directions, as is apparent from the particle velocities shown in Fig. 11(f).

Conclusions

Particle image velocimetry measurements in the wake of a hovering rotor were analyzed to better understand the turbulent nature of the flow as it interacted with a ground plane. The ultimate goal was to understand how the turbulent flow structures in the wake influence the process of sediment mobilization and uplift, hence leading to a better understanding of the problem of rotorcraft brownout. It was possible to assess the detailed nature of the boundary layer flow at the ground, showing that the mean flow comprised certain features of a turbulent wall jet, but only well downstream from the rotor. The instantaneous flow field was found to be much more complex and contained the remnants of the tip vortices, the vortex sheets from the rotor blades, and various other small scale turbulence and eddies. Dual-phase measurements have also been analyzed and the quadrant analysis method used to examine correlations between the turbulent motions in the carrier phase and the particle motion in the dispersed phase.

The following specific conclusions have been drawn:

1. The flow field at the ground below a hovering rotor comprises some features of a classical turbulent wall jet well away from the rotor. The validity of the logarithmic law of the wall between the viscous portion of the flow and the fully turbulent outer flow was shown to apply for the flow at the ground well downstream of the rotor.
2. Significant spatial variations were found in the important Reynolds shear stresses at the ground below the rotor, with the maximum shear stresses being located where the blade tip vortices approached closest to the ground, the vortices also inducing here the highest streamwise perturbation velocities.
3. In general, it was found that the Reynolds stresses in the boundary layer on the ground differed significantly from those measured in a fully developed turbulent boundary layer and a classical turbulent wall jet. The distribution of the Reynolds shear stress was not linear when moving away from the wall, and the fluctuations shown were attributed mainly to the action of the tip vortices and the turbulent vortex sheets from the rotor blade.
4. The results from the quadrant analysis suggested that this method has value for understanding the turbulence characteristics of complex rotor flows. A correlation was seen between the organized turbulent motions of the carrier phase and the movement and uplift of particles from the bed below the rotor. Although the results obtained thus far were very promising, more detailed dual-phase measurements with higher spatial resolution still need to be conducted and analyzed.

Acknowledgements

The Air Force Office of Scientific Research supported this work under a Multidisciplinary University Research Initiative, Grant W911NF0410176. The grant monitor was Dr. Douglas Smith. The authors would like to thank Dr. James Wallace and Mr. Robert Haehnel for their comments and suggestions on this work.

References

[1] Mapes, P., Kent, R., and Wood, R., "DoD Helicopter Mishaps FY85-05: Findings and Recommendations," U.S. Air Force, 2008.

[2] National Transportation Safety Board, NTSB Accident Briefs: LAX01LA283, LAX01LA304, LAX04LA285, SEA05CA173.

[3] Lee, T. E., Leishman, J. G., and Ramasamy, M., "Fluid Dynamics of Interacting Blade Tip Vortices With a Ground Plane," *Journal of the American Helicopter Society*, Vol. 55, 022005, 2010, DOI:10.4050/JAHS.55.022005.

[4] Milluzzo, J., Sydney, A., Rauleder, J., and Leishman, J. G., "In Ground Effect Aerodynamics of Rotors with Different Blade Tips, American Helicopter Society 66th Annual Forum Proceedings, Phoenix, AZ, May 10–13, 2010.

[5] Nathan, N. D., and Green R. B., "Measurements of a Rotor Flow in Ground Effect and Visualisation of the Brownout Phenomenon," American Helicopter Society 64th Annual Forum Proceedings, Montréal, Canada, April 29–May 1, 2008.

[6] Johnson, B., Leishman, J. G., and Sydney, A., "Investigation of Sediment Entrainment in Brownout Using High-Speed Particle Image Velocimetry," *Journal of the American Helicopter Society*, Vol. 55, 042003, 2010, DOI:10.4050/JAHS.55.042003.

[7] Sydney, A., Baharani, and A., Leishman, J. G., "Understanding Brownout Using Near-Wall High-Speed Dual-Phase Flow Measurements," American Helicopter Society 67th Annual Forum Proceedings, Virginia Beach, VA, May 3–5, 2011.

[8] Brown, R., and Whitehouse, G., "Modeling Rotor Wakes in Ground Effect," *Journal of the American Helicopter Society*, Vol. 49, (3), October 2004, pp. 238–249.

[9] Wenren, Y, Walter, J., Fan, M., and Steinhoff, J., "Vorticity Confinement and Advanced Rendering to Compute and Visualize Complex Flows," Paper AIAA-2006-945, 44th AIAA Aerospace Sciences Meeting and Exhibit, Reno, Nevada, January 9–12, 2006.

[10] Ryerson, C. C., Haehnel, R. B., Koenig, G. G., and Moulton, M. A., "Visibility Enhancement in Rotorwash Clouds," Paper AIAA-2005-263, 43rd AIAA Aerospace Sciences Meeting and Exhibit, Reno, NV, January 10–13, 2005.

[11] Haehnel, R. B., Moulton, M. A., Wenren, W., and Steinhoff, J., "A Model to Simulate Rotorcraft-Induced Brownout," American Helicopter Society 64th Annual Forum Proceedings, Montréal, Canada, April 29–May 1, 2008.

[12] Phillips, C., and Brown, R., "Eulerian Simulation of the Fluid Dynamics of Helicopter Brownout," American Helicopter Society 64th Annual Forum Proceedings, Montréal, Canada, April 29–May 1, 2008.

[13] D'Andrea, A., "Numerical Analysis of Unsteady Vortical Flows Generated by a Rotorcraft Operating on Ground: A First Assessment of Helicopter Brownout," American Helicopter Society 65th Annual Forum Proceedings, Grapevine, TX, May 27–29, 2009.

[14] Wachspress, D. A., Whitehouse, G. R., Keller, J. D., Yu, K., Gilmore, P., Dorsett, M., and McClure, K., "A High Fidelity Brownout Model for Real-time Flight Simulations and Trainers," American Helicopter Society 65th Annual Forum Proceedings, Grapevine, TX, May 27–29, 2009.

[15] Syal, M., Govindarajan, B., and Leishman, J. G., "Mesoscale Sediment Tracking Methodology to Analyze Brownout Cloud Developments," American Helicopter Society 66th Annual Forum Proceedings, Phoenix, AZ, May 10–13, 2010.

[16] Syal, M., and Leishman, J. G., "Comparisons of Predicted Brownout Dust Clouds with Photogrammetry Measurements," American Helicopter Society 67th Annual Forum Proceedings, Virginia Beach, Virginia, May 3–5, 2011.

[17] Mendoza-Cabrales, C., "Refined Modeling of Shallow, Turbulent Flow over Dunes," Ph.D. Dissertation, Colorado State University, Fort Collins, CO, 1987.

[18] McLean, S. R., and Smith, J. D., "A Model for Flow over Two-Dimensional Bed Forms," *Journal of Hydraulic Engineering*, Vol. 112, 1986, pp. 300–317.

[19] Nelson, J.M., Shreve, R. L., McLean, S.R., and Drake, T. G., "Role of Near-Bed Turbulence Structure in Bed Load Transport and Bed Form Mechanics," *Water Resources Research*, Vol. 31, 1995, pp. 2071–2086.

[20] Mulinti, R., and Kiger, K., "Two-Phase PIV Measurements of Particle Suspension in a Forced Impinging Jet," 63rd Annual Meeting of the APS Division of Fluid Dynamics, Vol. 55, (16), November 21–23, 2010, Long Beach, CA.

[21] Sechet, P., and Le Guennec, B., "The Role of Near Wall Turbulent Structures on Sediment Transport," *Water Resources Research*, Vol. 33, (17), 1999, pp. 3646–3656.

[22] Best, J., "On the Entrainment of Sediment and Initiation of Bed Defects: Insights from Recent Developments within Turbulent Boundary Layer Research," *Sedimentology*, Vol. 39, 1992, pp. 797–811.

[23] Ramasamy, M., Johnson, B., and Leishman, J. G., "Turbulent Tip Vortex Measurements Using Dual-Plane Stereoscopic Particle Image Velocimetry," *AIAA Journal*, 2009, Vol. 47, (8), pp. 1826–1840.

[24] Momayez, L., Dupont, P., and Peerhossaini, H., "Effects of Vortex Organization on Heat Transfer Enhancement," *International Journal of Thermal Sciences*, Vol. 43, (8), 2004, pp. 753–760.

[25] Syal, M., Rauleder, J., Tritschler, J. K., and Leishman, J. G., "On the Possibilities of Brownout Mitigation Using a Slotted-Tip Rotor Blade," 29th AIAA Applied Aerodynamics Conference, Honolulu, HI, June 27–30 , 2011.

[26] Bagnold, R. A., *The Physics of Blown Sand and Desert Dunes*, Dover Publications, Inc., Mineola, NY, 1941.

[27] Klebanoff, P. S., "Characteristics of Turbulence in a Boundary Layer with Zero Pressure Gradient," NACA Technical Report 1247, 1955.

[28] Hebbar, K. S., and Melnik, W. L., "Wall Region of a Relaxing Three-Dimensional Incompressible Turbulent Boundary Layer," *Journal of Fluid Mechanics*, Vol. 85, (1), 1978, pp. 39–48.

[29] Irwin, H. P. A. H., "Measurements in a Self-Preserving Plane Wall-Jet in a Positive Pressure Gradient," *Journal of Fluid Mechanics*, Vol. 61, (1), 1973, pp. 33–63.

[30] Wyganski, I., Katz, Y., and Horev, E., "On the Applicability of Various Scaling Laws to the Turbulent Wall Jet," *Journal of Fluid Mechanics*, Vol. 234, 1992, pp. 669–690.

[31] Geiser, J., and Kiger, K., "A Simplified Analog for a Rotorcraft-in-Ground-Effect Flow Using a Forced Impinging Jet," 63rd Annual Meeting of the APS Division of Fluid Dynamics, Vol. 55, (16), November 21–23, 2010, Long Beach, CA.

[32] Robinson, S. K., "Coherent Motions in the Turbulent Boundary Layer," *Annual Review of Fluid Mechanics*, Vol. 23, 1991, pp. 601–639.

[33] Purtell, L. P., Klebanoff, P. S., and Buckley, F. T., "Turbulent boundary layer at low Reynolds number," *Physics of Fluids*, Vol. 24, (5), 1981, pp. 802–811.

[34] Antonia, R. A., Bisset, D. K., and Browne, L. W. B., "Effect of Reynolds Number on the Topology of the Organized Motion in a Turbulent Boundary Layer," *Journal of Fluid Mechanics*, Vol. 213, 1990, pp. 267–286.

[35] Wallace, J. M., Eckelmann, H., and Brodkey, R. S., "The Wall Region in Turbulent Shear Flow," *Journal of Fluid Mechanics*, Vol. 54, 1972, pp. 39–48.